Giant magnetic anisotropy energy and coercivity in Fe island and atomic wire on W(110)

Takeshi Nakagawa,* Yasumasa Takagi, and Toshihiko Yokoyama
Institute for Molecular Science, and The Graduate University for Advanced Studies (Sokendai), Myodaiji-cho, Okazaki 444-8585, Japan

Torsten Methfessel, Sandra Diehl, and Hans-Joachim Elmers
Institut für Physik, Johannes Gutenberg-Universität Mainz, Staudingerweg 7, D-55099 Mainz, Germany
(Received 30 May 2012; published 25 October 2012)

We have directly investigated the giant magnetic anisotropy energy and coercivity of monolayer (ML) Fe islands and stripes on flat and stepped W(110) surfaces using x-ray magnetic circular dichroism. Both for islands and stripes, the magnetic anisotropy energy is ∼1.0 meV/atom, independent of the coverage below 0.5 ML. On the contrary, the coercive field of the islands rapidly drops from 4.3 T at 0.25 ML to 1.9 T at 0.50 ML, while that of the stripes moderately degrades from 3.5 T at 0.15 ML (∼3 atom rows) to 3.0 T at 0.50 ML. We explain the contrastive behavior for the islands and stripes by different nucleation and remagnetization processes. Considering the enhanced Fe moment, we find an unprecedented large value of the energy product $BH_{\max} = 5\ \mathrm{MJ/m^3}$.

DOI: 10.1103/PhysRevB.86.144418 PACS number(s): 75.70.Rf, 75.30.Gw, 75.50.Vv

I. INTRODUCTION

During the last decades, hard magnets have become an indispensable material both for data storage and power applications like electromotive actuators and power generators. Although the magnetic anisotropy energy and coercivity describe properties of magnetic materials, the energy product ($BH_{\max}$) characterizes hard magnets, which has improved in the last century more or less according to Moore's law. However, since 1990 rare earth (RE) magnets like $Nd_2Fe_{14}B$ have marked a saturation of the maximum available value of $BH_{\max} = 500\ \mathrm{kJ/m^3}$. Moreover, the replacement of the RE has been demanded due to the scarcity of RE, and novel approaches to improve hard magnets have attracted interest.[1]

Magnetic nanostructures with single atomic layers have a possibility to manifest prominent magnetic properties such as magnetocrystalline anisotropy energy (MAE) and coercivity that remarkably differ from the properties of bulk materials.[2–6] MAE originates from the anisotropy of the electronic structure, which is prominent in thin films due to low dimensionality and large strains. For nanostructures MAE and coercivity are crucial to stabilize magnetic states against thermal fluctuation. Coercivity is a complex property that is derived from the competition among MAE, domain wall creation, and structural defects.[7] The remagnetization process has two important scenarios: coherent rotation and domain wall nucleation followed by propagation. In the first case the coercivity is closely related to the MAE. Above a critical size of the nanostructure, the nucleation of a domain wall is more favorable and the coercivity decreases with increasing particle size.[8–11] For a cylindrical nanowire with an easy axis along the wire originating from the shape anisotropy, the coercivity decreases with the radius of the cylinder, as $\propto 1/r^2$.[12,13] However, the magnetic switching behavior for nanowires with a width of a few atomic rows has not been studied much.[14–17]

The Fe monolayer on W(110) has been extensively studied as an ideal two-dimensional ferromagnetic system with a pseudomorphic growth mode and a large strain. Its MAE of 0.55–8 meV has been evaluated from measurements of the domain wall width combined with a micromagnetic model,[3,10] which is supported by theoretical calculations.[18–20] Owing to its extremely large value, however, the anisotropy energy has not been directly determined from hard axis magnetization curves yet.

In this article, we have directly revealed the giant MAE as well as large coercivity in the Fe nanoislands and nanostripes grown on W(110). The MAE, which is approximately 1 meV/atom, does not depend on the shapes. The coercivity of the Fe islands with ∼15 nm reaches 4.3 T, and it decreases rapidly as the island size increases, which is in agreement with previous results.[8–11] On the other hand, the coercivity for the Fe nanowires is nearly constant with increasing the width, which has not been experimentally measured or theoretically predicted. We will discuss the shape-dependent coercivity based on the nucleation and domain wall propagation mechanism.

II. EXPERIMENTS

X-ray magnetic circular dichroism (XMCD) experiments were done at UVSOR-II 4B using elliptically polarized x-ray radiation with a degree of circular polarization of 65% at $T = 5$ K with a magnetic field of up to $B = 6$ T.[21] Spin-polarized scanning tunneling microscopy (SP-STM) was performed in a different chamber at $T = 5$ K and $B = 0$ T using W tips covered with (10 ± 1) ML Fe, sensitive to in-plane magnetization. W(110) substrates, a flat crystal, and a vicinal one with 2.7° miscut toward the $[1\bar{1}0]$ direction were cleaned in oxygen at 4×10^{-8} Torr at 1500 K and subsequently flashed at 2200 K. Fe islands were prepared on the flat substrate with the deposition at a substrate temperature of 300 K. Fe stripes were prepared on the stepped surface with a deposition at 300 K followed by annealing at 700 K, resulting in a step flow growth mode. For both XMCD and STM measurements, we employed the identical W substrates and similar Fe growth conditions, where the base pressures were below 1×10^{-10} Torr and Fe was deposited below 4×10^{-10} Torr. The quality of the samples was controlled by low-energy electron diffraction (LEED) observations.

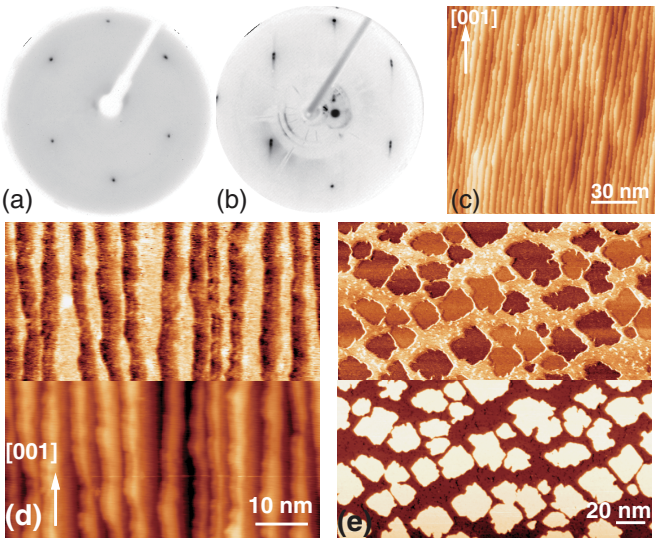

FIG. 1. (Color online) LEED patterns for (a) flat ($E_p = 100$ eV) and (b) stepped ($E_p = 85$ eV) surfaces. (c) An STM image on the stepped clean surface. (d) Topographic (lower) and nonmagnetic dI/dV (upper) maps for the stepped surface with $\Theta_{Fe} = 0.3$ ML ($U = 0.3$ V, $I = 0.6$ nA). (e) Topographic (lower) and spin-resolved (upper) STM images for $\Theta_{Fe} = 0.4$ ML on the flat surface ($U = 0.8$ V, $I = 1.5$ nA).

III. RESULTS AND DISCUSSION

The Fe nanostructures on flat and stepped W(110) crystals are shown in Fig. 1. Figures 1(a) and 1(b) show LEED patterns from the flat and stepped surfaces, respectively. The clear splitting of diffraction spots from the stepped surface proofs the regularity of the steps, which is directly visualized by STM [Fig. 1(c)]. The vicinal W(110) surface has a terrace width of (5 ± 2) nm, separated by steps of single atomic height, corresponding to the 20 atomic rows along the $[1\bar{1}0]$ direction. Fe atoms decorate the step edges and form monolayer (ML) stripes. Their width is proportional to the Fe coverage [Fig. 1(d)].[22] An Fe coverage, Θ_{Fe} (in units of pseudomorphic ML), of 0.05 ML corresponds to a nominal width of one atomic row. At a coverage close to 1 ML, the stripes begin to coalesce. Fe nanoislands grown on the flat surface have a variation of shapes. According to STM images, the average size of the islands increases with increasing coverage. We did not observe any domain walls in the islands at a remanent condition [Fig. 1(e)], and all the islands are magnetically single domain, in agreement with a previous report.[10]

XMCD measurements reveal magnetic moments, anisotropy, and coercivity for the Fe/W(110) nanostructures. Figure 2(a) depicts the experimental configurations, and Figs. 2(b)–2(d) show the x-ray absorption (XAS) and XMCD spectra for $\Theta_{Fe} = 0.25$ ML for three configurations where the incident directions for the x-ray light are 35° tilting from $[1\bar{1}0]$, [001] and normal to the surface, respectively. The background signal from the clean W(110) surface is subtracted from the spectra to apply the sum rules for spin and orbital magnetic moments.[23,24] The effective spin moments plotted in Figs. 2(e) and 2(f) include the contribution from the

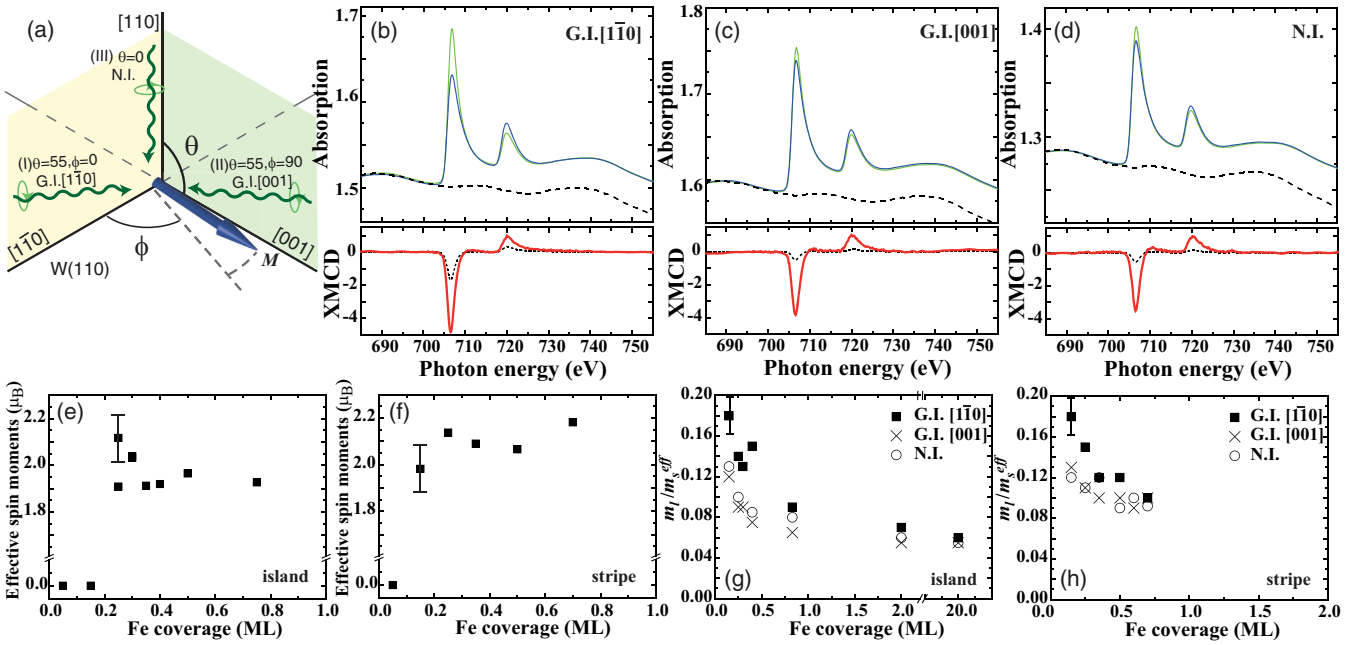

FIG. 2. (Color online) (a) Experimental configurations for XMCD. The polar (θ) and azimuthal (ϕ) angles are measured from the [110] and $[1\bar{1}0]$ directions, respectively. Two grazing (G.I. $[1\bar{1}0]$ and G.I. [001]) incidences and a normal (N.I. [110]) incidence are employed. The photon beam and the magnetic field are in parallel. (b)–(d) XAS and XMCD spectra for $\Theta_{Fe} = 0.25$ ML Fe on a W(110) flat taken at $T_s = 5$ K and $B = \pm 5$ T. The dashed lines in XAS represent the background signal from the clean W(110) surface. In XMCD the dashed lines show the XMCD spectra normalized to the edge jump, while the solid lines normalized to the height of the L_2 edge. (e), (f) Effective spin moments for Fe islands (e) and stripes (f) as determined at a remanent condition. (g), (h) Ratio between orbital moments and effective spin moments on the flat (g) and the stepped (h) surfaces.

magnetic dipolar operator. Using a d hole number of 3.4 and the obtained magnetic moments in the remanent state, where the magnetization is confined in the (110) surface along the [1$\bar{1}$0] direction, the spin magnetic moment for Fe is evaluated to be $(1.98 \pm 0.1)\mu_B$ for the islands and $(2.08 \pm 0.1)\mu_B$ for the stripes The total moment (m) including the orbital moment below 1 ML is 2.2–2.4μ_B, in rough agreement with the magnetization determined by classical magnetometry (2.5μ_B).[25] The obtained total magnetic moment at 0.25 ML is 2.3–2.4μ_B, which is enhanced compared to that for bulk bcc Fe (2.2μ_B). Enhanced total magnetic moments are found in submonolayer films, which is mainly caused by the nonvanishing orbital moment in the broken symmetry.[4,6,17,26] Below $\Theta_{Fe} = 0.25$ ML for islands and $\Theta_{Fe} = 0.15$ ML for stripes, no remanent magnetization is observed, indicating a breakdown of the ferromagnetic state or a huge coercivity above $B = 6$ T. The XMCD spectra for the grazing incidence (G.I.) [1$\bar{1}$0] show a larger L_3 peak compared to those for G.I. [001] and normal incidence (N.I.) [110], which evidences a larger orbital moment along the [1$\bar{1}$0] direction, coinciding with the easy axis.[22] Figures 2(g) and 2(h) show the ratios between the orbital (m_l) and the effective spin moments ($m_s^{\rm eff}$) for Fe islands and stripes, respectively. With increasing Fe coverage, the ratio $m_l/m_s^{\rm eff}$ decreases.

For both systems $m_l/m_s^{\rm eff}$ decreases rapidly and approaches the bulk value even at $\Theta_{Fe} = 1$ ML. Possible origins of the large orbital moment for the lower Fe coverage are the epitaxial strain and the lower coordination number. The strain could modify the orbital moment, but for Fe/W(110) it gives smaller impacts because the epitaxial strain, the in-plane lattice constant, does not change throughout the pseudomorphic Fe layer, having 1 × 1 registry on W(110) both for the Fe islands and nanowires.[27] The increased orbital moment in this case is mainly caused by the perimeter Fe atoms.[4,6,26]

In order to evaluate the anisotropy and coercivity, we measured magnetization loops by recording white line intensities at the Fe L_3 edge as a function of the magnetic field. Figure 3(a) shows magnetization curves at $\Theta_{Fe} =$ 0.25 ML on the flat W(110) surface. The magnetic curves are measured in the three configurations as used for the XMCD measurements [Fig. 2(a)]. The magnetization is normalized using the evaluation by the sum rule analysis of the XMCD results at $B = \pm 5$ T, where the magnetization along the hard axes is approximately 30% of the saturation value. The magnetization curve along G.I. [1$\bar{1}$0] at $\Theta_{Fe} = 0.5$ ML in Fig. 3(c) reveals that the larger Fe islands are remagnetized under the approximately half magnetic field compared to that for the island at $\Theta_{Fe} = 0.25$ ML. On the other hand, for the Fe nanostripes, the remagnetization field at $\Theta_{Fe} = 0.25$ ML in Fig. 3(b) does not differ much from that at $\Theta_{Fe} = 0.50$ ML in Fig. 3(d).

The MAE is calculated using a first-order approximation for the surface anisotropy contribution to the free enthalpy. We formulate the free enthalpy per Fe atom, $F(\theta,\phi) = c_1 \cos^2\theta + c_2 \sin^2\theta \sin^2\phi - \boldsymbol{m} \cdot \boldsymbol{B}$, where θ and ϕ are the angles defined in Fig. 2(a). Figures 3(e) and 3(f) show the anisotropy constants c_1 and c_2, representing the out-of-plane ([110]) and the in-plane ([001]) anisotropies. The obtained anisotropy energy along [110] involves the contribution from the shape anisotropy, $\mu_0 M^2/2 = 0.09$ meV, for the islands

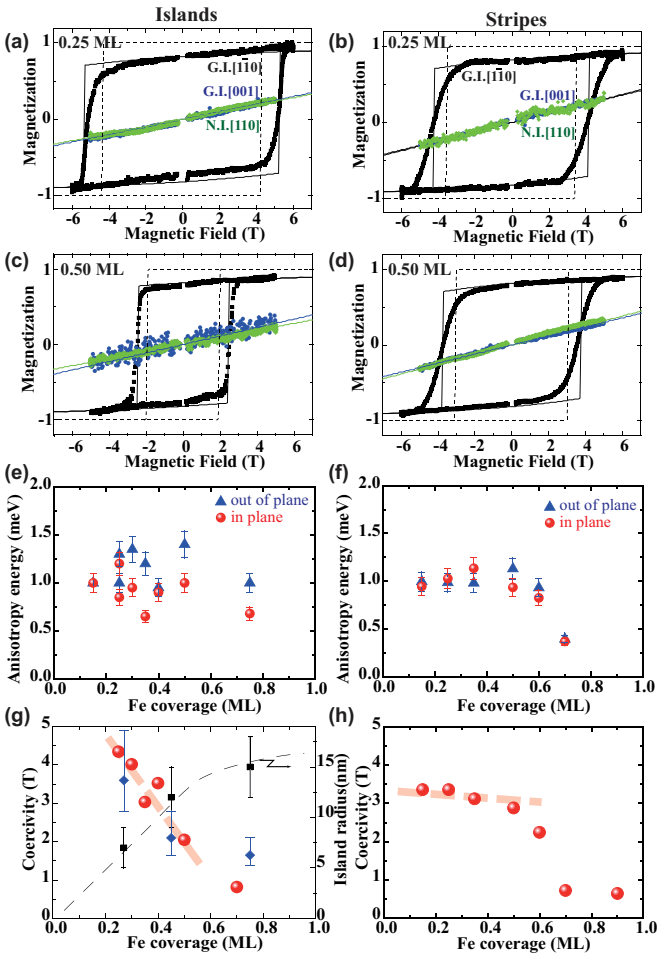

FIG. 3. (Color online) Magnetization curves, magnetic anisotropy energy (MAE), and coercivity for Fe islands and stripes. (a) Magnetization curves of Fe islands ($\Theta_{Fe} = 0.25$ ML) on W(110) for the three configurations [see Fig. 2(a)]. The solid lines are results of the magnetization anisotropy model. The dashed lines show magnetization curves, assuming that the magnetic field is along the [1$\bar{1}$0] direction. See text for details. (b) The same as (a), but for the Fe stripes on stepped W(110) surfaces. (c), (d) Magnetization curves for (c) the Fe island ($\Theta_{Fe} = 0.50$ ML) and (d) the Fe stripe ($\Theta_{Fe} = 0.50$ ML). (e), (f) MAE for (e) the Fe islands and (f) stripes. The triangles and the circles represent the anisotropies for [110] (out-of-plane) and [001] (in-plane) directions, respectively. (g) Coercivity for Fe islands as a function of Θ_{Fe}. Circles shows experimental results, while the diamonds are obtained by the magnetization reversal model. The island size is also shown by the squares. The dashed lines are guides for the eye. (h) Coercivity for the Fe nanostripes as a function of Θ_{Fe}.

studied. After the correction of the shape anisotropy, the MAE along [110] is 1.1 meV/atom for $\Theta_{Fe} = 0.25$ ML and shows slight deviation with increasing Fe coverage. The MAE along [001] is 1.3 meV/atom at $\Theta_{Fe} = 0.25$ ML. With increasing Fe coverage, the MAE slightly decreases, reaching 0.5 meV/atom at $\Theta_{Fe} = 1$ ML. The MAE of 1 meV/atom in combination with $m = 2\mu_B$ corresponds to an anisotropy field of 17.3 T, which is huge for typical ferromagnetic materials.[28] The value of 1 meV/atom corresponds to 1×10^7 J/m^3, which is comparable to the value for $Nd_2Fe_{14}B$ (5×10^6 J/m^3) and

3 orders of magnitude larger than bulk Fe (5×10^4 J/m^3). The anisotropy energy for the Fe stripes is plotted in Fig. 3(f), displaying a similar behavior. For the Fe stripes, the obtained anisotropy energy along the [110] and [1$\bar{1}$0] directions involves the contribution from the shape anisotropy, corresponding to 0.02 and 0.07 meV/atom for $\Theta_{\mathrm{Fe}} = 0.15$ ML. The MAE is nearly constant up to $\Theta_{\mathrm{Fe}} = 0.6$ ML, but it drops to 0.5 meV/atom at $\Theta_{\mathrm{Fe}} = 0.7$ ML. This reduction may originate from the starting of the second layer, which is judged from the observation of hysteresis along the surface normal.[3] Both for islands and stripes in the ferromagnetic state, the MAE shows an almost constant value below $\Theta_{\mathrm{Fe}} = 0.6$ ML.

The coercivities obtained for the Fe nanoislands and stripes are shown in Figs. 3(g) and 3(h), respectively. All the islands and stripes in this study remagnetize by the domain wall scenario[10] because the coercive field is less than 1/3 of the anisotropy field (∼17 T), even for the highest value. In the case of coherent rotation, the coherent rotation model theoretically predicts that the remagnetization occurs at the field equal to the anisotropy field at low temperatures,[7,28] which does not hold for the Fe/W(110) system in this study. The coercivities are evaluated using the first-order approximation combined with energy barriers, since XMCD could not be performed with the magnetic field parallel to the easy axis [1$\bar{1}$0] direction. The energy barriers are introduced to simulate the measured hysteresis curves under the G.I. [1$\bar{1}$0] condition as demonstrated in Figs. 3(a)–3(d), which evaluates coercivities via an inhomogeneous magnetization state different from the coherent rotation. For the islands, the coercivity is 4.3 T at $\Theta_{\mathrm{Fe}} = 0.25$ ML, which is extraordinarily large even among magnetic thin films. Its BH_{max} product amounts to 5.0 MJ/m^3 for $\Theta_{\mathrm{Fe}} = 0.25$ ML. No hysteresis loops were observed below 0.2 ML. With increasing Fe coverage, the coercivity of the Fe islands rapidly decreases and drops to 1.9 T at $\Theta_{\mathrm{Fe}} = 0.5$ ML. For the Fe stripes, hysteresis loops appear for $\Theta_{\mathrm{Fe}} \geqslant 0.15$ ML with a coercive field of 3.4 T. With increasing Fe coverage, the coercivity moderately decreases to 3.0 T at 0.5 ML. Above $\Theta_{\mathrm{Fe}} = 0.7$ ML, the coercivity rapidly degrades below 1 T.

A giant coercive field is expected to correlate with a large MAE. The observed MAE values are comparable both for the Fe islands and stripes and do not show any significant variation below 0.6 ML. In contrast, the coercivity shows a clear difference between the islands and the stripes as a function of Θ_{Fe}. The overall large coercivity can be traced back to the large MAE both along the [001] and [110] directions, because the easy and the intermediate axes define the plane of magnetization rotation. For single magnetic domains, the magnetization reversal proceeds either via coherent rotation or by domain wall nucleation and propagation. Due to the giant MAE in Fe/W(110), the domain wall is narrow, i.e., the width is on the order of a few nanometers or less,[3,10] and it can nucleate in an island with 10-nm diameter. When the size of the island decreases down to the width of the domain wall, the switching is realized by coherent rotation, which occurs well below 0.15 ML for Fe/W(110).

In the following, we discuss the temperature dependence of the coercivity. In our study we measured the coercivity above $\Theta_{\mathrm{Fe}} = 0.25$ ML, where the Fe islands consists of more than 2000 atoms. The total anisotropy energy is more than 1 eV, which is much larger than $k_B T = 5 \times 10^{-4}$ eV. Even with the reduced barrier height for switching by the domain wall creation, $E_B \simeq m\mu_0 H_c$, the coercivity of 4.3 T at 5 K increases slightly to 4.7 T at 0 K by a temperature-dependent model.[29] Therefore we neglect the temperature-induced reduction of the coercivity at 5 K for $\Theta_{\mathrm{Fe}} > 0.25$ ML.

The coercivity of the islands and the stripes shows a different dependence on Θ_{Fe}. This variation can be explained by the different mechanisms of the domain wall creation. Assuming the domain wall energy as γ_{DW} and the width of Fe stripe along the [1$\bar{1}$0] direction as w, the energy loss due to the domain wall is $\gamma_{\mathrm{DW}} w$. The domain wall energy is expressed as $4\sqrt{AK}$, where A is the exchange stiffness and K is the anisotropy energy.[7] When the magnetic field increases, the associated energy barrier per Fe atom decreases due to the magnetostatic energy $m\mu_0 H$. At the coercive field $\mu_0 H_c$, the energy loss by the domain wall should be balanced with the energy gain in the reversed domain $2Nwm\mu_0 H_c$, where N is the initial nucleation width. This leads to a width-independent coercivity $\mu_0 H_c = \gamma_{\mathrm{DW}}/2Nm$, assuming that γ_{DW} is independent of the stripe width, which is reasonable since the anisotropy and the spin moment do not change drastically below 0.6 ML. With $\gamma_{\mathrm{DW}} = 15$ meV (Ref. 30) and $\mu_0 H_c = 3$ T, N is estimated to be 20 atoms. Thus the constant domain energy and MAE in the Fe stripe result in a constant coercivity.

The coercivity of the island can also be obtained from the energy balance between domain wall formation and magnetostatic energy. For large nanoparticles in which domain walls can spread out, an energy barrier for the reversal decreases as inversely proportional to its radius, $1/r$.[8,10,11] Obviously the Fe islands on W(110) show a similar trend. Let us consider the shape of the Fe islands as circles with their radius r for simplicity. At $\mu_0 H_c$, the domain wall has to expand across the island in order to overcome the highest energy cost and the energy gain due to the magnetization reversal is $2m\mu_0 H_c \pi r^2/2C$, where C is the area per single Fe atom. Taking the total domain wall energy as $2r\gamma_{\mathrm{DW}}$, the resulting coercivity is $\mu_0 H_c = 4C\gamma_{\mathrm{DW}}/\pi rm$. The coercivity is proportional to $1/r$. Figure 3(g) shows the calculated coercivity using the island size obtained by STM. The calculated $\mu_0 H_c$ values are in agreement with the experimental results. There is a deviation between the experimental and calculated results for $\Theta_{\mathrm{Fe}} > 0.5$ ML, which is due to the appearance of an interaction between the islands[22] and the coalescence of the islands. Assuming that the Fe islands linearly enlarge as the Fe coverage increases, $\pi r^2 \propto \Theta_{\mathrm{Fe}}$, the coercivity is proportional to $1/\sqrt{\Theta_{\mathrm{Fe}}}$. When the shape of the Fe island deviates from a circle, r should be replaced by the longest atomic rows along the [1$\bar{1}$0] direction and the number of the reversed Fe atoms by the correct one.[10] This modification does not change the result drastically.

In conclusion, we have directly evaluated the giant MAE and coercivity in Fe islands and stripes on W(110). The MAE is approximately 1 meV/atom along the [001] and [110] directions, which is in agreement with previous estimations. Although Fe islands and stripes exhibit similar MAE, a remarkable difference is found in the coercivity. A nearly constant coercivity in the Fe stripes is explained by the domain

wall model, which suggests a constant energy barrier height for the nanostripes with their magnetization perpendicular to the wire direction. The Fe islands exhibit a much larger coercivity for smaller sizes and show a drastic decrease with increasing the size. The shape-dependent coercivity in the magnetic monolayer revealed in this work will play a key role in tuning magnetic properties.

ACKNOWLEDGMENTS

This research was partially supported by a Grants-in-Aid for Scientific Research (KAKENHI) (No. 23710136 and No. 22241029) and the Sokendai Overseas Research Program. S.D. is a recipient of a fellowship through the Excellence Initiative (DFG/GSC 266).

*nakagawa@ims.ac.jp

[1]H. Zeng, J. Li, J. P. Liu, Z. L. Wang, and S. Sun, Nature (London) **420**, 395 (2002).
[2]H. J. Elmers, J. Hauschild, H. Höche, U. Gradmann, H. Bethge, D. Heuer, and U. Köhler, Phys. Rev. Lett. **73**, 898 (1994).
[3]M. Pratzer, H. J. Elmers, M. Bode, O. Pietzsch, A. Kubetzka, and R. Wiesendanger, Phys. Rev. Lett. **87**, 127201 (2001).
[4]P. Gambardella, S. Rusponi, M. Veronese, S. S. Dhesi, C. Grazioli, A. Dallmeyer, I. Cabria, R. Zeller, P. H. Dederichs, K. Kern, C. Carbone, and H. Brune, Science **300**, 1130 (2003).
[5]P. Gambardella, A. Dallmeyer, K. Maiti, M. C. Malagoli, W. Eberhardt, K. Kern, and C. Carbone, Nature (London) **416**, 301 (2002).
[6]P. Ohresser, N. B. Brookes, S. Padovani, F. Scheurer, and H. Bulou, Phys. Rev. B **64**, 104429 (2001).
[7]A. Hubert and R. Schäfer, *Magnetic Domains* (Springer, Berlin, 2008).
[8]E. F. Kneller and F. E. Luborsky, J. Appl. Phys. **34**, 656 (1963).
[9]W. F. Brown, Phys. Rev. **130**, 1677 (1963).
[10]S. Krause, G. Herzog, T. Stapelfeldt, L. Berbil-Bautista, M. Bode, E. Y. Vedmedenko, and R. Wiesendanger, Phys. Rev. Lett. **103**, 127202 (2009).
[11]S. Ouazi, S. Wedekind, G. Rodary, H. Oka, D. Sander, and J. Kirschner, Phys. Rev. Lett. **108**, 107206 (2012).
[12]E. H. Frei, S. Shtrikman, and D. Treves, Phys. Rev. **106**, 446 (1957).
[13]W. Wernsdorfer, B. Doudin, D. Mailly, K. Hasselbach, A. Benoit, J. Meier, J. P. Ansermet, and B. Barbara, Phys. Rev. Lett. **77**, 1873 (1996).
[14]P. Gambardella, A. Dallmeyer, K. Maiti, M. C. Malagoli, S. Rusponi, P. Ohresser, W. Eberhardt, C. Carbone, and K. Kern, Phys. Rev. Lett. **93**, 077203 (2004).
[15]J. Shen, R. Skomski, M. Klaua, H. Jenniches, S. S. Manoharan, and J. Kirschner, Phys. Rev. B **56**, 2340 (1997).
[16]X. D. Ma, T. Nakagawa, Y. Takagi, M. Przybylski, F. M. Leibsle, and T. Yokoyama, Phys. Rev. B **78**, 104420 (2008).
[17]H. Fujisawa, S. Shiraki, M. Furukawa, S. Ito, T. Nakamura, T. Muro, M. Nantoh, and M. Kawai, Phys. Rev. B **75**, 245423 (2007).
[18]T. Andersen and W. Hübner, Phys. Rev. B **74**, 184415 (2006).
[19]A. T. Costa, R. B. Muniz, J. X. Cao, R. Q. Wu, and D. L. Mills, Phys. Rev. B **78**, 054439 (2008).
[20]L. Udvardi and L. Szunyogh, Phys. Rev. Lett. **102**, 207204 (2009).
[21]T. Nakagawa, Y. Takagi, Y. Matsumoto, and T. Yokoyama, Jpn. J. Appl. Phys. **47**, 2132 (2008).
[22]J. Hauschild, H. J. Elmers, and U. Gradmann, Phys. Rev. B **57**, R677 (1998).
[23]P. Carra, B. T. Thole, M. Altarelli, and X. Wang, Phys. Rev. Lett. **70**, 694 (1993).
[24]B. T. Thole, P. Carra, F. Sette, and G. van der Laan, Phys. Rev. Lett. **68**, 1943 (1992).
[25]H. J. Elmers, G. Liu, and U. Gradmann, Phys. Rev. Lett. **63**, 566 (1989).
[26]S. Rusponi, T. Cren, N. Weiss, M. Epple, P. Buluschek, L. Claude, and H. Brune, Nature Mater. **2**, 546 (2003).
[27]M. Albrecht, U. Gradmann, T. Reinert, and L. Fritsche, Solid State Commun. **78**, 671 (1991).
[28]R. C. O'Handley, *Modern Magnetic Materials* (Wiley-Interscience Publications, New York, 1999).
[29]S. Rohart, V. Repain, A. Tejeda, P. Ohresser, F. Scheurer, P. Bencok, J. Ferré, and S. Rousset, Phys. Rev. B **73**, 165412 (2006).
[30]M. Pratzer and H. J. Elmers, Phys. Rev. B **67**, 094416 (2003).